Sea ice edge automatic retrieval based on morphology

WANG Weibo, SU Jie

Key Laboratory of Physical Oceanography, MOE, Ocean University of China, Qingdao 266100, *China*

Abstract: Sea ice edge is an important index for illustrating changes in the Arctic sea ice. This parameter is important for navigation safety and sea ice disaster warning in Chinese northern coast. Sea ice edge is often previously obtained through long-term artificial judgment or in default equivalent to a certain isoline of sea ice concentration, which neglects the influence of large floes on sea ice edge. This study aims to develop a more accurate and faster automatic method for monitoring sea ice edge compared with conventional monitoring techniques. A novel method based on morphology is proposed. Connected Component Analysis (CCA) and image closing operation are performed. The main ice region, main water region, and floes are distinguished using CCA twice. Then, some large floes are reserved and merged into the principal ice region. Finally, sea ice edge is retrieved by a changeable image closing operation with self-adaptive structural element. This method can be extensively applied to ice-water binary data, such as sea ice concentration, satellite image, and aerial image. The proposed technique is applied on the reflectance data produced from band 1 and band 2 of MODIS (Moderate-resolution Imaging Spectroradiometer). The new method is used to retrieve sea ice edge from sea ice concentration data from advanced microwave scanning radiometer for EOS data covering ten regions in the Arctic ocean. Compared with the 15% isoline of sea ice concentration in the regions covered by many large ice floes, the sea ice edge obtained by the new method is more reasonable for monitoring large-scale sea ice. This advantage is caused by the reservation and merging of slightly large floes into the principal ice region. Rapid monitoring of sea ice in the Chinese northern coast without the restriction of chosen data formatis feasible because the method is automatic and can be widely applied. Meanwhile, the dramatic change in the Arctic sea ice can be quantified using the sea ice edge obtained by the proposed method. A regional and integral Arctic sea ice edge dataset can be built for further Arctic studies.

Key words: sea ice edge retrieval method, changeable image closing operation, connected component analysis

CLC number: TP701 **Document code:** A

Citation format: **Wang W B and Su J. 2015. Sea ice edge automatic retrieval based on morphology. Journal of Remote Sensing, 19(6): 983-997 [DOI: 10.11834/jrs.20154121]**

1 INTRODUCTION

Air sea heat exchange occurs between ocean and atmosphere when sea ice is completely cut off. Great deviation in air sea interaction is presented among regions covered by sea ice and open sea water. Sea ice edge represents the boundary of sea ice with open water; thus, the accurate determination of the edge is significant to understand the considerable decrease in sea ice.

The most common data resource for determining sea ice edge has been recently derived from sea ice concentration datasets. To date, retrieval algorithms involving sea ice concentration are mainly developed on the basis of microwave and visible-near-infrared (VIS-NIR) remote sensing data. Microwave remote sensing is not influenced by clouds, but it has low resolution (generally more than 4 km). VIS or NIR remote sensing exhibits higher resolution (e.g., the resolution of AVHRR is 1.1 km, that of MODIS is 250 m, and that of Landsat is only 30 m). However, these techniques are easily influenced by cloud, fog, and perpetual nightin the polar region. Many recent retrieval algorithms of sea ice concentration using microwave data (Comiso, 1990; Cavalieri, et al., 1990; Spreen, et al., 2008; Su, et al., 2013; Hao & Su, 2015) and VIS-NIR data (Drue & Heinemann, 2005) can provide the corresponding Arctic-Antarctic sea ice concentration products. The sea ice concentrations produced from the aforementioned operational satellite data can provide enormous initial data for retrieving the sea ice edge.

Sea ice edge is defined as the envelope of the principal sea ice region. Partial small floes are ignored in the identification of sea ice edge. The change in sea ice edge position can be used to reveal the daily, seasonal, or annual extent of the variation in sea ice. For example, Worby, et al. (1998) indicated that the storm system in the Antarctic can cause daily shift of ice edge up to 1° latitude. Variation in the sea ice edge is apparent because of the melting sea ice. Mu and Zhao (2013) analyzed the daily sea ice concentration from microwave data. They showed that the maximum offshore distance of the sea ice edge in Green land Sea

Received: 2014-05-21; **Accepted:** 2015-04-25; **Version of record first published:** 2015-05-02

Supported by National Natural Science Foundation of China (No. 41330960); State Oceanic Administeration Public Welfare Project (No. 201105016); National Basic Research Program of China (973 Program) (No. 2010CB951403)

First author biography: WANG Weibo (1986—), male, he majors in ocean optics. E-mail: wangwb@tio.org.cn

Corresponding author biography: SU Jie (1966—), female, her current research includes sea ice remote sensing and ice ocean coupling. E-mail: sujie@ouc.edu.cn

decreased annually during winter from 2003 to 2011, whereas the minimum offshore distance increased in autumn. Divine, et al. (2004) constructed a time series of ice edge in Nordic Seas during 1750—2002 and showed oscillations of ice cover with periods of about 60—80 and 20—30 years. Sea ice edge is an important parameter for marine ecosystems (Sullivan, et al., 1988), offshore maritime traffic safety, and offshore oil platform. In China, the offshore distance of sea ice edge is the sole criterion for sea ice disaster warning.

Ice-water boundary can be identified on the basis of the different physical properties between sea water and sea iceas shown in satellite images. Brevik, et al. (2011) used advanced scatterometer (ASCAT) C-band data to determine the ice-water boundary. This multisensory analytical method, in which ASCAT and SSM/I 85 GHz data are imported and SSM/I 19 and 37 GHz data are used as a filter, was implemented and monitored fora year. Finally, daily sea ice boundary with a 10 km grid was obtained. Previous retrieval methods of sea ice edge were often implemented through hartificial judgment, human-computer interaction, or automatic identification from sea ice concentration. Artificial judgment suggests that the sea ice edge should be directly retrieved from sea ice charts by human eye. Artificial judgment was still retained, although Mahoney, et al. (2008) presented the criteria of landfast, drift, and multiyear ice edges. Artificial method and human-computer interaction are often accompanied by highly subjective judgments, which may reduce work efficiency. Automatic retrieval is widely applied because of its direct determination of sea ice edge from sea ice concentration. For example, sea ice edge is often defined as an isoline of sea ice concentration of 15% (Worby, et al., 1998; Worby & Comiso, 2004; Ogi, et al., 2008; Mu and Zhao, 2013) or 30% (Divine and Dick, 2006). This technique results in coarse sea ice edge, which needs further processing because many separate floes have been ignored. Worby and Comiso (2004) showed that the sea ice edge observed from a ship during the ice growth season (March-October) in the Antarctic sea ishighly consistent-with satellite images of the sea ice edge obtainedusing the isoline methodin the same period. However, a low agreement was observed with the sea ice edge detected using apassive microwave radiometer during the melting season (November-February). Anerror of 1°—2° latitude was obtained. Wang, et al. (2011) avoided the misjudgment caused by the reflectance of sediment in the Bohai Sea by distinguishing ice and water from MODIS data with the agglomerative hierarchical clustering method and by retrievingsea ice edge withthe Sobel edge detection method. This method does not consider size when determining whether or not a floe is reserved. However, the reserved floe is separated from the main sea ice region in the retrieval of sea ice edge.

Reasonable retrieval of the sea ice edge from the ice region mostly covered byfloes is important. The ideal retrieval of sea ice edge is as follows. Fair-sized floes are initially chosen and merged into the principal sea ice region. The sea ice edge is retrieved from the merged sea ice data. The merged data are then processed using severalsome image operation methods, such as Connected Component Analysis (CCA) and image closing operation. This paper reports a simple, automatic, and novel method without human-computer interaction to retrieve sea ice edge.

2 DESCRIPTION ON METHOD

2.1 Principle of method

The proposed retrieval method utilizes CCA and image closing operation. CCA is an important technique in image processing and contains three steps: (1) utilization of Connected Component Labeling (CCL), (2) acquisition of the shape characteristic of each connected component, and (3) determination of the grayscale characteristic of each connected component. In the first step, all subsets of connected components are found according to a given regulation and uniquely labeled by different signs. CCL is the most important among the three steps. Pixel- and block-based algorithms in CCL are used in this study.

The pixel-based algorithm has a subset of connected components with a known pixel labeled according to a given regulation. The 8-adjacency connectivity is adopted in this study. This process is used to determine whether or not eight adjacent pixels have the same value with a known pixel and to save pixels that meet the regulation. The pixels inside the dotted line in Fig. 1 have similar values. Then, the connected pixels based on the saved pixels are explored in accordance with the 8-adjacency connectivity regulation. The algorithm is terminated until no connected pixel is reached. The collection of connected pixels is named as a connected component.

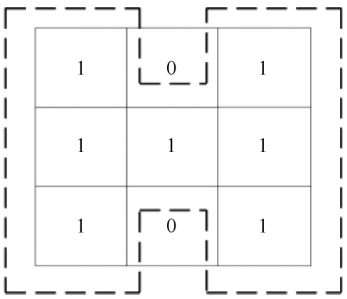

Fig. 1 Diagram of 8-adjacency connectivity

The block-based algorithm focuses on an area or image, in which all subsets of connected components are labeled based on the 8-adjacency connectivity regulation. The connected component is labeled by one value, and unconnected components are labeled by different values. In this process, the first pixel is operated using the pixel-based algorithm, and its connected component is labeled by, for example, (1) Progressive scan is not performed until a pixel not equal to the first labeled value is found. Then, its connected component is labeled as (2) By analogy, all pixels in the area are labeled.

Image closing operation is importantin image processing and involveserosion and dilation operations. The basic effect of dilation operation on a binary image is to gradually enlarge the boundaries of regions of foreground pixels. Thus, areas of foreground pixels grow in size, whereasholes within these regions become smaller. The dilation of the binary image A by the structuring element $\boldsymbol{B}$ is defined by $\boldsymbol{A} \oplus \boldsymbol{B} = \mathrm{U}\{\boldsymbol{A} + b : b \in \boldsymbol{B}\}$. The basic effect of erosion operation on a binary image is to erode the boundary of region of foreground pixels. Thus, areas of foreground pixels shrink in size, and holes within those areas become

larger. This process is mathematically expressed as $\boldsymbol{A} \otimes \boldsymbol{B} = \mathrm{I}\{\boldsymbol{A} + b : b \in \boldsymbol{B}\}$. Image closing operation is defined simply as a dilation followed by an erosion using the same structuring element for both operations. This process is mathematically expressed as $(\boldsymbol{A} \oplus \boldsymbol{B}) \otimes \boldsymbol{B}$. The operator preserves the background regions that have a similar shape to the structuring element or that can completely contain the structuring element while eliminating all other regions of background pixels (Zheng & Ye, 1997).

CCL is used to label pixels that possess similar properties and that are connected to each other. This technique can be used in sea ice researchto distinguish the ice region from the sea water region. Thus, the characteristic of polynya distribution can be retrieved (Fu, et al., 2012; Chen, et al., 2012). Erosion operation can eliminate small floes, and dilation operation can connect the adjacent floes. Hence, the closing operation can connect fair-sized floes with the principal ice region without changing theice coverage.

2.2 Changeable image closing operation

An appropriate structuring element is crucial in the closing operation. A small structuring element induces the disconnection of the ice region from with other floes. By contrast, a large structuring element consumes much time and resources as well as reduces work efficiency. A changeable closing operation has been developed, in which a suitable structuring element has been applied. Detailed information will be discussed inthenext section. This particular 3×3 structuring element in erosion and dilatation is commonly used and regarded as the initial matrix of $\boldsymbol{B}$, that is, $\begin{bmatrix} 0 & 1 & 0 \\ 1 & 1 & 1 \\ 0 & 1 & 0 \end{bmatrix}$. The changeable structuring element may be altered in agreement with the shape of the following matrix (Eq. (1)).

$$\boldsymbol{B} = \begin{bmatrix} 0 & 0 & \cdots & 1 & \cdots & 0 & 0 \\ 0 & \cdots & 1 & 1 & 1 & \cdots & 0 \\ \cdots & 1 & 1 & 1 & 1 & 1 & \cdots \\ 1 & 1 & 1 & 1 & 1 & 1 & 1 \\ \cdots & 1 & \cdots & 1 & 1 & 1 & \cdots \\ 0 & \cdots & 1 & 1 & 1 & \cdots & 0 \\ 0 & 0 & \cdots & 1 & \cdots & 0 & 0 \end{bmatrix}_{m \times m} \quad (1)$$

2.3 Flow of method

The sea ice edge retrieval method in this study is based on ice-water binary data. In theory, the method can be used in any dataset, for example, sea ice concentration data, satellite image, or aerial image. We introduce aretrieval process of sea ice edge by using the MODIS Band-1 reflectance data with a resolution of 250 km on the 114th day in 2001 in Bering Sea. Data coverage is shown in Fig. 2. Data are converted into binary format by using the strength ratio algorithm proposed by Zhao & Ren (2000). The retrieval of sea ice edge is shown in Fig. 3. Detailed information is as follows.

Step 1 Binarization of satellite image. The selected high-latitude area should be covered by sea ice, and the low-latitude area should be covered by open water (Fig. 2). The reflectance value in MODIS band-1 is between 0 and 1. The threshold value is obtained as the cutoff value of sea ice compared with sea water. A pixel with a value higher than the threshold is regarded as ice and labeled as 1, whereas a pixel with a value lower than the threshold is regarded as sea water and labeled as 0. The results are shown in Fig. 4(a).

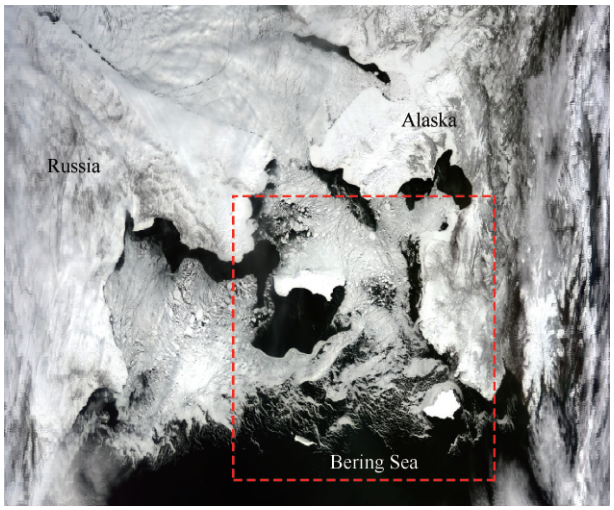

Fig. 2 True color map of Bering Sea using MODIS band 1 data on 114th Julian day, 2001
(Data in red box were selected for retrieving sea ice edge)

Step 2 Determination of ice and water reference pixels. We selected a certain ice pixel (e. g., the first image pixel) located at a high latitude as the ice reference pixel P_i and a certain sea water pixel (e. g., the final image pixel) located at a low latitude as the water reference pixel P_w.

Step 3 Retrieval of the main water region. Detailed information is based on the obtained binary data. A subset of connected components with a known sea water pixel P_w is obtained using the pixel-based algorithm and named as the main water region. Finally, each connected component is labeled as 1, and the other region is labeled as 0 (Fig. 4(b)).

Step 4 Retrieval of the main ice region. Similar to step 3 and based on the result of step 3, a subset of connected components with a known ice pixel P_i is obtained and named as the main ice region. Each connected component is labeled as 1. Other pixels are labeled as 0 (Fig. 4(c)).

Step 5 Acquisition of floes. Two images of similar values obtained by step (3) (4) areregarded as floes separated from the main ice region, as shown by white pixels in Fig. 4(d).

Step 6 Elimination of small floes merging into the main ice region and acquisition of the basic ice region. Different floes are labeled by natural numbers when the block-based algorithm is used to analyze the result of step 5. The number of pixels in afloe is counted to select fair-sized floes with more than β pixels that would be labeled as1. The chosen floes and main ice region are regarded as the basic ice region. Thus, the number of the separate subset of connected component is $n+1$ (n is the number of floes). The fair-sized floes are shown in Fig. 4(d), and the basic ice region is shown in Fig. 4(e).

Step 7 Utilization of the changeable closing operation. The basic ice region is handled by the changeable closing opera-

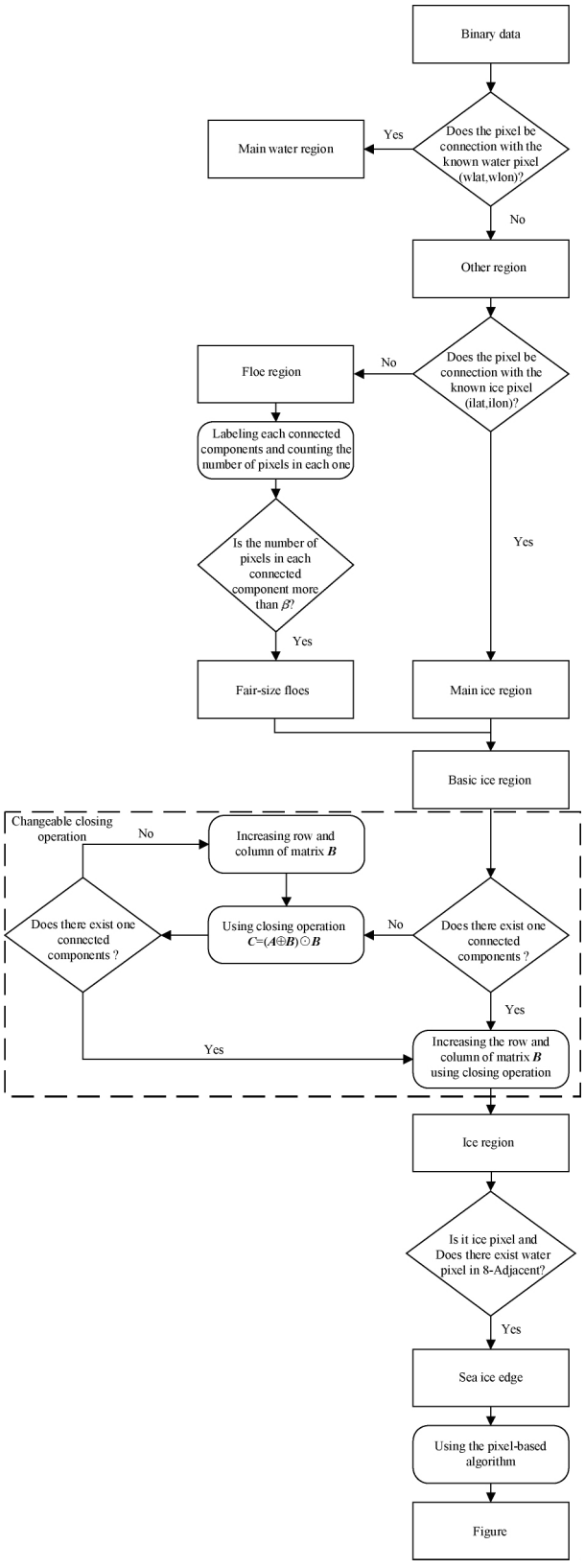

Fig. 3 Flow chart of retrieved sea ice edge by changeable image closing operation

tion. Detailed information is as follows. The basic ice region is operated by closing the operation with the initial structuring element. If the number of connected components is 1, the process is terminated. Otherwise, the process is continued. The basic ice region is operated again by closing the operation and increasing the number of columns and rows by 2. The process is not terminated until the number of connected components is 1. The sea ice edge is smoothened by continuing four other instances of changeable closing operation when the structuring element is also changed, similar to the above process in each instance. Finally, only the connected components are labeled as 1, and the other pixels are labeled as 0.

Step 8 Determination of the position of sea ice edge. The result from step 7 is handled according to 8-adjacency connectivity. The ice pixel around which a water pixel exists in the 8-adjacency pixels is regarded as the sea ice edge pixel and labeled as 1. Other pixels are labeled as 0.

Step 9 Exporting the continuous position of sea ice edge. The result from step 8 is handled using the pixel-based algorithm. The sea ice edge is visualized by exporting the position of the sea ice edge in accordance with the format of BLN file. Detailed information about the BLN file can be found in http://www.goldensoftware.com/. Finally, the sea ice edge is illustrated in Fig. 4(f).

Thus, the automatic retrieval of sea ice edge involves the binarization of data, the use of CCL to identify the main ice and main water regions, the selection of fair-sized floes, the merging into the main region, and finally the acquisition of the ice region. Then, the changeable closing operation is used to produce a connected component. Finally, sea ice position information is retrieved from the only connected component.

3 APPLICATION AND ANALYSIS

Sea ice edge can be easily retrieved from sea ice concentration data using the proposed method, because the proposed method is based on binary data. Binary data can be established by setting up the threshold value. A pixel with sea ice concentration more than the threshold is considered as sea ice and labeled as 1, and a pixel with sea ice concentration less than the threshold is considered as sea water and labeled as 0.

In this context, threshold values of 0% and 15% are chosen, and two sea ice edges are retrieved using the proposed method and marked by green and red lines (Fig. 5).

The sea ice edge, defined as the 15% isoline (blue line), is unreasonable in partial regions (Fig. 5). For example, the isoline is discontinuous at the location of polyny as labeled by A. Two separate closed loops are present at the location marked by B. The sea ice edge retrieved using the proposed method with the threshold value of 0% (green line) is remote from the principal sea ice region. This condition can be attributed to the fact that some zonal ice regions, such as the ice tongue, are frequently produced and extended to the open water region during the melting season because of the action of wind to sea ice (Fig. 5). When the threshold value is 0%, the sea ice edge (green line) retrieved using the new method is the line connecting the ends of the zonal ice regions. The interior of this type of sea ice edge contains a certain amount of open water regions connected to the outer sea. Compared with the result of the 0% threshold, the sea ice edge (red line) retrieved by the proposed method with the 15% threshold represents the principal sea ice region better.

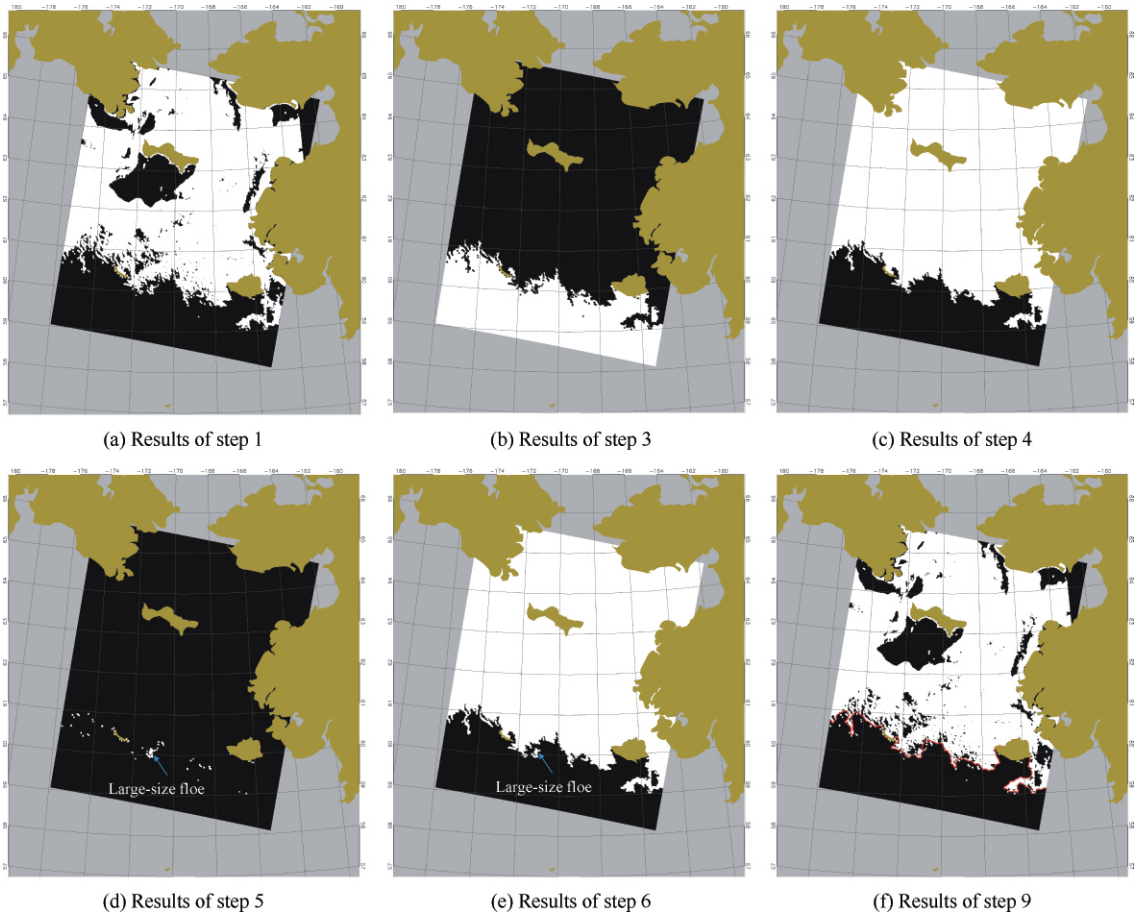

(a) Results of step 1 (b) Results of step 3 (c) Results of step 4

(d) Results of step 5 (e) Results of step 6 (f) Results of step 9

Fig. 4 Process diagram of retrieved sea ice edge by changeable image closing operation

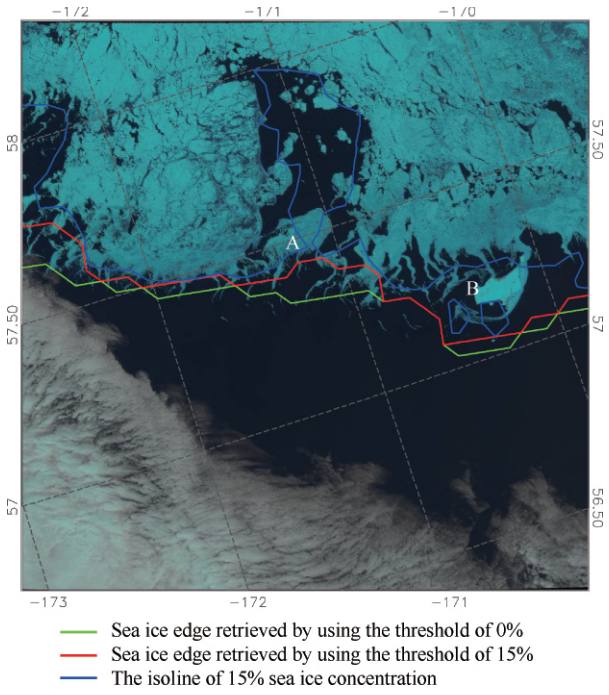

Fig. 5 Sea ice edges retrieved from ice-water binary data produced using the threshold of 0% and 15%, respectively, from AMSRE (advanced microwave scanning radiometer for EOS) sea ice concentration data for April 19, 2013 (The background is the true color satellite image produced from real-time Landsat data)

We select 15% as the threshold and obtain the sea ice edge through the flow path shown in Fig. 3. The advanced microwave scanning radiometer for EOS (AMSRE) sea ice concentration data with a resolution of 6.25 km are obtained from Su, et al. (2013). Ten examples located in different areas and at different times are shown in Fig. 6(a)—Fig. 6(j). Some specified regions, such as regions covering many small floes (e.g., E1), large floes (e.g., E2), and the leads (e.g., E3), have been labeled by the alphabet and following number. We compare the results obtained using the proposed method with that of the 15% isoline of sea ice concentration. A small difference was found between the sea ice edge sand the 15% isoline in the ice region with a few floes (Fig. 6(c), Fig. 6(g), and Fig. 6(h)). The obtained sea ice edges are smooth. A remarkable difference was found between the sea ice edges located in the ice region with a dramatic change in sea ice concentration (Fig. 6(a), Fig. 6(b), Fig. 6(d), Fig. 6(e), Fig. 6(f), Fig. 6(i), and Fig. 6(j)). In ice regions covering many small floes, as labeled by A1, D1, E1, and J1 for example, these 15% isolines are coarse, and many small individual connected components are found.

Compared with the 15% isolines, the sea ice edges retrieved by the new method still maintain several floes and eliminate most floes. In ice regions with large floes, as indicated by D1, E2, F1, I1, and J2 in Fig. 6, the ice edge of the large floes is separated from the main ice edgeobtained using the isoline method. In the proposed method, large floes are merged into the main ice region and then the sea ice edge is retrieved. In leads, as labeled by B1, B2, E3, and I2, the 15% isoline is

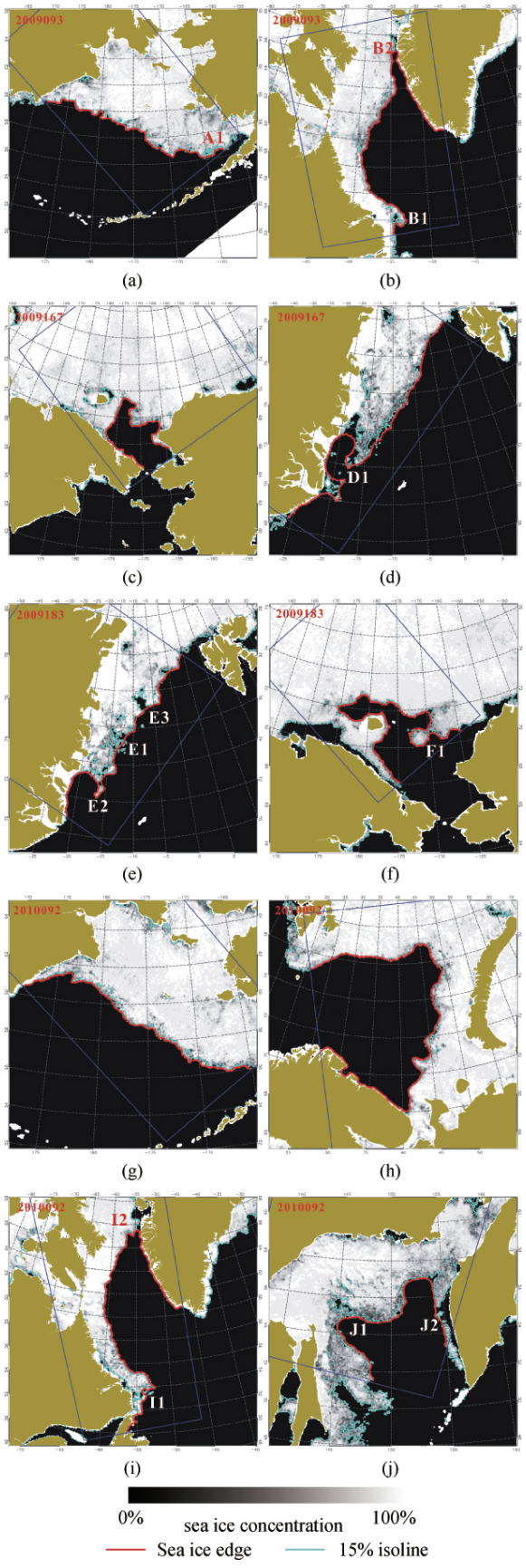

Fig. 6 Comparison between sea ice edge retrieved by changeable image closing operation and the 15% isoline

(A—J are the sea ice concentration distribution in different Arctic region, The blue box denotes the range of selected data)

along the lead. The obtained sea ice edge is connected at the mouth of the lead and is in agreement with the concept of the extent of traditional large-scale sea ice.

We present intuitively the difference between two types of sea ice edge obtained by the new and isoline methods in Fig. 6. The new method is found to be advantageous. Landsat data only cover land and inshore area; thus, they cannot be used for comparison and verification in whole sea area, for example, Bering Sea. Therefore, we cannot quantify the difference between the two types of sea ice edge obtained by the proposed method, such as the red line in Fig. 6, and sea ice edge obtained through the new method from Landsat data (not shown in Fig. 6) to illustrate the precision of improvement. We can probably explore a new indicator in future studies from other efficient data to show the advantage of the new method.

4 CONCLUSIONS

Sea ice edge can visually express sea ice extent and is important in Arctic research. In China, sea ice edge is also used as the only indicator for sea ice disaster warning. Thus, an automatic and efficient method for retrieving sea ice edge should be developed. A simple and efficient method of retrieving sea ice edge has been developed to eliminate the subjectivity in artificial judgment and reserve fair-sized floes. The method is based on CCL and closing operation. This method can be widely applied in any binary dataset containing sea ice concentration, aerial sea ice image, or satellite sea ice image.

The proposed method was used to retrieve sea ice edges located in 10 regions and at different times from AMSRE sea ice concentration data. A small difference was found between the 15% isoline and the ice region covering a few floes. However, differences still exist in the ice region covering floes with varied sizes. On the one hand, retrieving sea ice edge using the new method eliminated several small floes. On the other hand, fair-sized floes were merged into the main ice region. The obtained sea ice edge can be used to efficiently measure the change in the extent of large-scale sea ice.

The proposed method is automatic, efficient, simple, and can be extensively applied. Thus, this method can be used in acquiring large-scale, real-time, or long time-scale sea ice edge to improve sea ice forecast and research.

Acknowledgements: We greatly appreciate Guang huaHao and Yanqing Li for providing the AMSRE sea ice concentration data and Yuguang Liu for providing some suggestions for the revision.

REFERENCES

Breivik L A, Eastwood S and Lavergne T. 2012. Use of C-Band scatterometer for sea ice edge identification. IEEE Transactions on Geoscience and Remote Sensing, 50(7): 2669 – 2677 [DOI: 10.1109/TGRS.2012.2188898]

Cheng Y Y, Shi J X and Zheng S J. 2012. Temporal and spatial variation of the Mackenzie Bay Polyna, Antarctic and its main impact factors. Periodical of Ocean University of China, 42(7/8): 1 – 9

Divine D V and Chad D. 2006. Historical variability of sea ice edge posi-

tion in the Nordic Seas. Journal of Geophysical Research, 111: C01001 [DOI: 10.1029/2004JC002851]

Drüe C and Heinemann G. 2005. Accuracy assessment of sea-ice concentrations from MODIS using in-situ measurements. Remote sensing of Environment, 95(2): 139 - 149 [DOI: 10.1016/j.rse.2004.12.004]

Fu H L, Zhao J P and Frey K E. 2012. Investigation of polynya dynamics in the northern Bering Sea using greyscale morphology image-processing techniques. International Journal of Remote Sensing, 33(7): 2214 - 2232 [DOI: 10.1080/01431161.2011.608088]

Hao G H and Su J. 2015. A study on the dyramic tie points ASI algorithm in the Arctic Ocean. Acta Oceanologica Sinica, 34(11): 54 - 64

Key J and Haefliger M. 1992. Arctic ice surface temperature retrieval from AVHRR thermal channels. Journal of Geophysical Research: Atmospheres (1984—2012), 97(D5): 5885 - 5893 [DOI: 10.1029/92JD00348]

Kong B. 2003. A fast connected component analysis algorithm and its implementation. PR & AI, 16(1): 110 - 115

Liu C L and Zhao J P. 2013. Pack ice extent and its spatiotemporal variation in summer Arctic. Acta Oceanologica Sinica, 35(4): 36 - 46

Mahoney A R, Barry R G, Smoolyanitsky V and Fetterer F. 2008. Observed sea ice extent in the Russian Arctic, 1933—2006. Journal of Geophysical Research, 113: C11005 [DOI: 10.1029/2008JC004830]

Mu L J and Zhao J P. 2013. Variability of the Greenland sea ice edge. Advances in Earth Science, 28(6): 709 - 717 [DOI: 10.11867/j.issn.1001 - 8166.2013.06.0709]

Ogi M, Rigor I G, McPhee M G and Wallace J M. 2008. Summer retreat of Arctic Sea Ice: role of summer winds. Geophysical Research Letters, 35(24): L24701 [DOI: 10.1029/2008GL035672]

Spreen G, Kaleschke L and Heygster G. 2008. Sea ice remote sensing using AMSR-E 89-GHz channels. Journal of Geophysical Research (Oceans), 113(C2) [DOI: 10.1029/2005JC003384]

Su J, Hao G H, Ye X X and Wang W B. 2013. The experiment and validation of sea ice concentration AMSR-E retrieval algorithm in polar region. Journal of Remote Sensing, 17(3): 495 - 513 [DOI: 10.11834/jrs.20132043]

Sullivan C W, McClain C, Comiso J C and Smith W O Jr. 1988. Phytoplankton standing crops within an Antarctic ice edge assessed by satellite remote sensing. Journal of Geophysical Research, 93(C10): 12487 - 12498 [DOI: 10.1029/JC093iC10p12487]

Wang N, Zhang X, Ji Y G, Lu T Z and Yu B. 2011. A method of MODIS sea ice edge extraction based on agglomerative hierarchical clustering method. Journal of Geo-Information Science, 13(2): 266 - 272 [DOI: 10.3724/SP.J.1047.2011.00266]

Worby A P and Comiso J C. 2004. Studies of the Antarctic sea ice edge and ice extent from satellite and ship observations. Remote Sensing of Environment, 92(1): 98 - 111 [DOI: 10.1016/j.rse.2004.05.007]

Worby A P, Massom R A, Alllison I, Lytle A I and Heil P. 1998. East Antarctic sea ice: a review of its structure, properties and drift//Jeffries M O, ed. Antarctic Sea Ice: Physical Processes, Interactions and Variability. Antarctic Research Series (Book 74). American Geophysical Union: 41 - 67 [DOI: 10.1029/AR074p0041]

Zhao J P and Ren J P. 2000. Study on the method to analyze parameters of arctic sea ice from airborne digital imagery. Journal of Remote Sensing, 4(4): 271 - 278 [DOI: 10.11834/jrs.20000406]

Zheng L and Ye D T, 1997. Application of grey-scale mathematical morphology methods to fundus image processing. Journal of Tsinghua University (Sci & Tech), 37(4): 76 - 80

基于形态学的海冰外缘线自动提取

王维波，苏洁

中国海洋大学 物理海洋教育部重点实验室，山东 青岛 266100

摘 要: 海冰外缘线是一个描述北极海冰快速变化的重要指示参数,对近岸冰区航行保障和海冰灾害预警具有实际意义。本文首先基于形态学中的方法分别识别数据中的主体冰域、主体水域和碎冰区。其次利用可变图像闭运算方法将较大碎冰与主体冰区合并,最后再利用连通域方法提取海冰外缘线。该方法可适用于任何冰水二值数据集,包括海冰密集度产品数据、卫星图像、航拍图像以及其他冰水混合数据。本文基于 AMSR-E 海冰密集度数据,利用此方法提取了北冰洋 10 个区域的海冰外缘线,与 15% 海冰密集度等值线比较表明,本文方法能够保留较大面积的碎冰区域,并将其与主体冰域合并处理,因此所提取的海冰外缘线在衡量大尺度海冰范围方面更为合理。

关键词: 海冰外缘线,可变图像闭运算,连通域,北极,海冰密集度

中图分类号: TP701 文献标志码: A

引用格式: 王维波,苏洁. 2015. 基于形态学的海冰外缘线自动提取. 遥感学报,19(6): 983 - 997

Wang W B and Su J. 2015. Sea ice edge automatic retrieval based on morphology. Journal of Remote Sensing, 19(6): 983 - 997 [DOI: 10.11834/jrs.20154121]

1 引 言

海冰是大气和海洋之间的隔绝层,限制着海气之间热量交换。海冰的隔绝作用导致冰区和开阔水域的海气相互作用存在巨大差别。海冰外缘线作为描述冰区和开阔水域的分界线,正确的识别海冰外缘线对理解北极海冰快速变化非常重要。

目前,研究海冰最有效的数据来源于卫星遥感获得的海冰密集度数据。至今,海冰密集度的反演技术已较为成熟,主要包括基于微波数据的反演技术和基于可见光和红外光的反演技术,其中微波数据受云雾影响小,但分辨率较低; 可见光和红外光分辨率较高(如 AVHRR 数据为 1.1 km,MODIS 数据最高分辨率可达 250 m,Landsat 数据分辨率为 30 m) ,但是受极夜和云雾的影响(Key 和 Haefliger,1992) 。目前针对微波数据(Spreen 等,2008; 苏洁等,2013; Hao 和 Su,2015; http://nsidc.org/data/nsidc-0051; http://nsidc.org/data/NSIDC-0079) 和可见光数据(Drüe 和 Heinemann,2005) 的海冰密集度的反演算法已有很多研究,两种数据各有特点,都能提供结冰海区的海冰密集度。这些海冰密集度数据为提取海冰外缘线提供了巨大的数据来源。

海冰外缘线定义为海冰主体的包络线,忽略了数量不多的零星海冰。海冰外缘线位置的变化能直观地反映海冰的年际以及季节变化规律,也是研究海冰变化规律的一个重要参数。例如 Worby 等人(1918) 发现南大洋气旋能够使海冰外缘线位置的变化超过 1°。近年,在北极快速变化的背景下,海冰外缘线变化比以往更加明显。牟龙江依据微波遥感日海冰密集度数据发现 2003 年—2011 年格陵兰海冬季海冰外缘线离岸距离极大值逐年减小,而夏季海冰外缘线离岸距离极小值却逐年增大(牟龙江和赵进平,2013) 。Divine 和 Dick(2006) 发现 1750 年—2002 年的 4 月—8 月北欧海海冰外缘线位置存在 60—80 年和 20—30 年的年代际震荡变化,其中格陵兰海海冰外缘线主要表现出低频变化,而巴伦支海表现出高频变化。他们认为近年北

收稿日期: 2014-05-21; 修订日期: 2015-04-25; 优先数字出版日期: 2015-05-02

基金项目: 国家重点基础研究发展计划(973 计划) (编号: 2013CBA01800) ; 国家自然科学重点基金项目(编号: 41330960) ; 国家海洋局公益项目(编号: 201105016)

第一作者简介: 王维波(1986—) ,男,助理研究员,从事极区物理海洋学和海洋光学方面研究,E-mail: wangwb@tio.org.cn

通信作者简介: 苏洁(1966—) ,女,副教授,现从事冰海耦合与海冰遥感方面研究,E-mail: sujie@ouc.edu.cn

欧海海冰外缘线退缩可能是海冰外缘线位置 60—80 年的年代际震荡的表现。海冰外缘线位置对生态(Sullivan 等, 1988)、近海海上交通安全和石油平台作业也具有重要的实用价值。

通过海冰密集度或冰水物理性质差异可以准确判识冰水交界,如 Breivik 等人(2012)第一次将 C 波段散射计(ASCAT)数据引入到海冰外缘线识别当中,同时融合 SSM/I 89 GHz 数据,将 SSM/I 19 GHz 和 37 GHz 作为滤波器,利用贝叶斯分类方法,得到了分辨率为 10 km 的日冰水交界网格数据。提取海冰外缘线的位置通常可以采用人工、人机交互形式或基于海冰密集度自动确定。人工识别是直接采用人眼观测的方式从图像数据中获得海冰外缘线位置信息。Mahoney 等人(2008)曾给出了沿岸冰外缘线、流冰外缘线和多年冰外缘线的判断标准,并在此基础上加入人工判识确定各类冰的外缘线。人工或人机交互方式方法带有较大的主观性,而且由于大量烦琐而重复的工作而降低工作效率。以往的海冰外缘线自动判别方法一般是基于海冰密集度等值线直接确定,如将海冰冰外缘线定义为海冰密集度 15% 的等值线(Worby 等,1998,Worby 和 Comiso,2004,Ogi 等,2008,牟龙江和赵进平,2013)或 30% 的等值线(Divine 和 Dick,2006)。这种方法比较粗糙,而且由于海冰外缘区存在大量琐碎的浮冰,判别出的海冰外缘线不光滑,也不够准确。(Worby 和 Comiso)2004 发现海冰密集度 15% 等值线与利用船基观测的南极海冰外缘线的位置冬季差别不大,但是在夏季,存在约 1°—2°的偏差,并且指出两者之间的差别可能是不同数据集计算得到的南极夏季海冰面积差别很大的原因(Worby 和 Comiso, 2004)。为了去除泥沙效应引起的可见光数据对海冰的误判,王宁等人(2011)首次将凝聚层次聚类方法引入到 MODIS 冰水识别算法中,并利用 Sobel 算子提取海冰外缘线,该算法通过碎块大小阈值控制是否保留碎冰,使碎冰独立于主体冰区。

合理提取碎冰区海冰外缘线是非常困难的,同时也是不能忽视的。在提取海冰外缘线的过程中,经常采用将碎冰区忽略的处理方法,例如舍去海冰密集度为 15% 以下的海冰格点,以 15% 等值线所在位置视为海冰外缘线(Worby 等,1998,Worby 和 Comiso,2004,Ogi 等,2008,牟龙江和赵进平,2013),或采用判断碎冰大小,选择性保存大块碎冰并独立提取海冰外缘线的方法(王宁 等,2011)。最理想的处理过程应该是选择较大的碎冰区,将其和主体冰区融合,并根据融合得到的海冰区域提取海冰外缘线。本文正是基于此思路,利用图像处理中连通域和图像闭运算方法,提出了一种简单可行的、不需要进行人机交互方式的海冰外缘线的自动提取方法。

2 算法研究

2.1 算法的原理

本文提出的海冰外缘线提取算法运用了图像处理中连通域分析方法 CCA(Connected Component Analysis)和图像闭运算(Closing Operation)方法。

连通域分析是图像分析中一个重要的方法,包括三部分:(1)连通域标记 CCL(Connected Component Labeling),即在规定的连通性规则下,给每一个物体或目标分配一个唯一的非零标号;(2)计算每一个连通域的形状特征;(3)计算每一个连通域的灰度特征。其中连通域标记是最重要的步骤,是后两部分计算的基础(孔斌,2003)。在本文中主要使用两种方法进行连通域标记:单点连通域标记和区域连通域标记。

单点连通域标记是已知某点特征,依据连通规则,寻找与它特征相同的且连通点的集合。本文所述的连通规则采用的是 8 邻域连通,即每个格点与其周围的 8 个点进行连通,如图 1 所示,其中虚线包含的点性质相同。在进行连通域标记时,对给定点与周围 8 个点进行识别,保存性质相同的点,然后对这些相同性质的点的周围 8 个点继续进行识别。直到找不到性质相同的点为止。所有性质相同点的集合,标记为一个连通域。

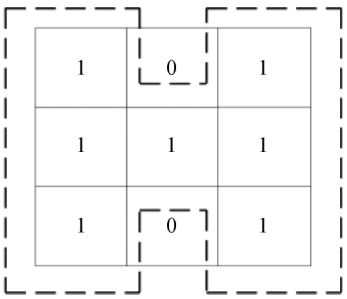

图 1 8 邻域连通示意图

区域连通域标记的处理对象是整个图像区域,是对性质相同且连通的点标记,不连通的区域采用

不同值进行标记的方法。如果连通域标记是按照自然数标记,那么标记号即为图像中连通域的个数。该方法同样采用 8 个邻域连通方式,采用了"经典方法"处理遥感图像(孔斌,2003)。方法如下:首先对图像第一个数据点进行单点连通域标记,例如标记为 1。然后逐行扫描像素点,直到找到标记不为 1 的像素点,标记为 2,再次使用单点连通域标记,以此类推,直到整个图像像素点都被标记为止。

图像闭运算也是图像分析中一个重要方法,其中包括图像的膨化算法和腐蚀算法。膨化算法是将与目标点接触的背景点合并到该目标物中,是目标边界向外界扩张的处理方法。膨化算法可以用来填补目标区域中存在的空洞,消除目标区域内的小颗粒噪声。膨化算法的算符为⊕,数学表达式为:$A \oplus B = \mathrm{U}\{A + b : b \in B\}$,其中 B 为结构元素,决定着膨化方向。腐蚀算法是一种消除边界点,使边界向内收缩的过程。可以用来消除小且无意义的目标物。腐蚀算法的算符为⊗。数学表达式:$A \otimes B = I\{A + b : b \in B\}$,$B$ 为结构元素,决定着腐蚀方向。图像的闭运算,是将上述膨化算法和腐蚀算法结合在一起,使用同一个结构元素对图像先膨化再进行腐蚀的运算。闭运算数学表达式为$(A \oplus B) \otimes B$。闭运算通常用于填补目标内细小的空洞,连接断开的邻近目标,平滑其边界的同时并不明显改变面积(郑玲和叶大田,1997)。

图像处理算法中连通域算法能标记相同性质的点。在海冰研究中,能够提取水域和冰域。依据这一特点,前人成功地识别了冰间湖分布特征(Fu 等,2012,程瑶瑶 等,2012)。腐蚀算法能够去除小碎冰区域(Fu 等,2012,程瑶瑶 等,2012),膨化算法能够连接断开的邻近海冰。结合两者的特点,本文给出的图像闭运算算法能在不明显改变面积的情况下,将碎冰和主体冰域相连。

2.2 可变图像闭运算方法的提出

在图像闭运算算法中,选择合适的结构元素 B 是非常重要的。如果结构元素 B 选择太小,主体冰域将不能连接碎冰。如果选择太大,图像处理将消耗大量时间,而降低工作效率。基于图像闭运算的特点,本文提出了可变图像闭运算方法,即自动选择合适的结构元素。具体实施步骤将在下面算法流程中详细介绍。需要指出的是,本文给出的结构元素 B 依据式(1)矩阵特征变化,初始值设为 3×3 矩阵 $\begin{bmatrix} 0 & 1 & 0 \\ 1 & 1 & 1 \\ 0 & 1 & 0 \end{bmatrix}$。

$$B = \begin{bmatrix} 0 & 0 & \cdots & 1 & \cdots & 0 & 0 \\ 0 & \cdots & 1 & 1 & 1 & \cdots & 0 \\ \cdots & 1 & 1 & 1 & 1 & 1 & \cdots \\ 1 & 1 & 1 & 1 & 1 & 1 & 1 \\ \cdots & 1 & L & 1 & 1 & 1 & \cdots \\ 0 & \cdots & 1 & 1 & 1 & \cdots & 0 \\ 0 & 0 & \cdots & 1 & \cdots & 0 & 0 \end{bmatrix}_{m \times m} \quad (1)$$

2.3 算法的流程

本文提出的海冰外缘线提取方法是基于冰水二值场数据,原理上适用于任何数据集,包括海冰密集度产品数据,卫星图像以及其他冰水混合数据。这里以北极太平洋扇区海冰外缘线为例,基于 2001 年第 114 天分辨率为 250 m 的 MODIS1B 通道 1 的反照率数据,选取的数据区域如图 2 所示,利用强度比算法(赵进平和任敬萍,2000;刘成龙和赵进平,2013),生成的冰水二值场数据。海冰外缘线提取流程图如图 3 所示。

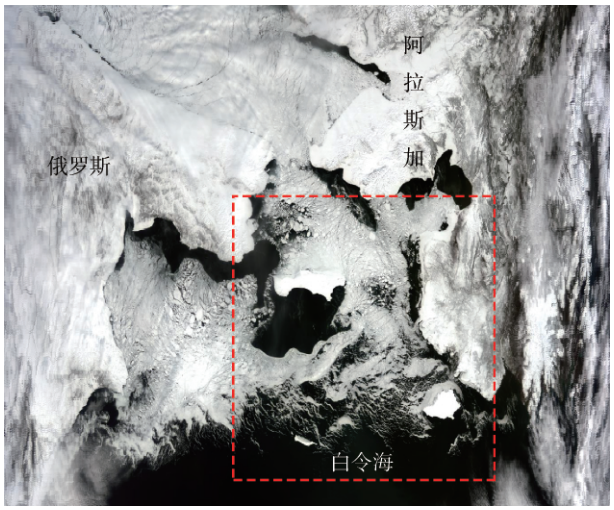

图 2 2001 年第 114 天的 MODIS 真彩图
(红框为本文选取的数据范围)

海冰外缘线提取算法实现的具体步骤如下:

步骤 1:利用强度比方法对图像进行二值化处理。选取的数据要求高纬度为大面积冰区,低纬度为大面积水域。MODIS 通道 1 反照率数据为 0—1 之间的数值。基于反照率数据利用强度比方法能方便地找出海水和海冰的分界反照率 α。数据中反照率如果小于 α,则被认为是水点,记为 0;如果值大于 α,则被认为是冰点,记为 1,如图 4(a)所示。

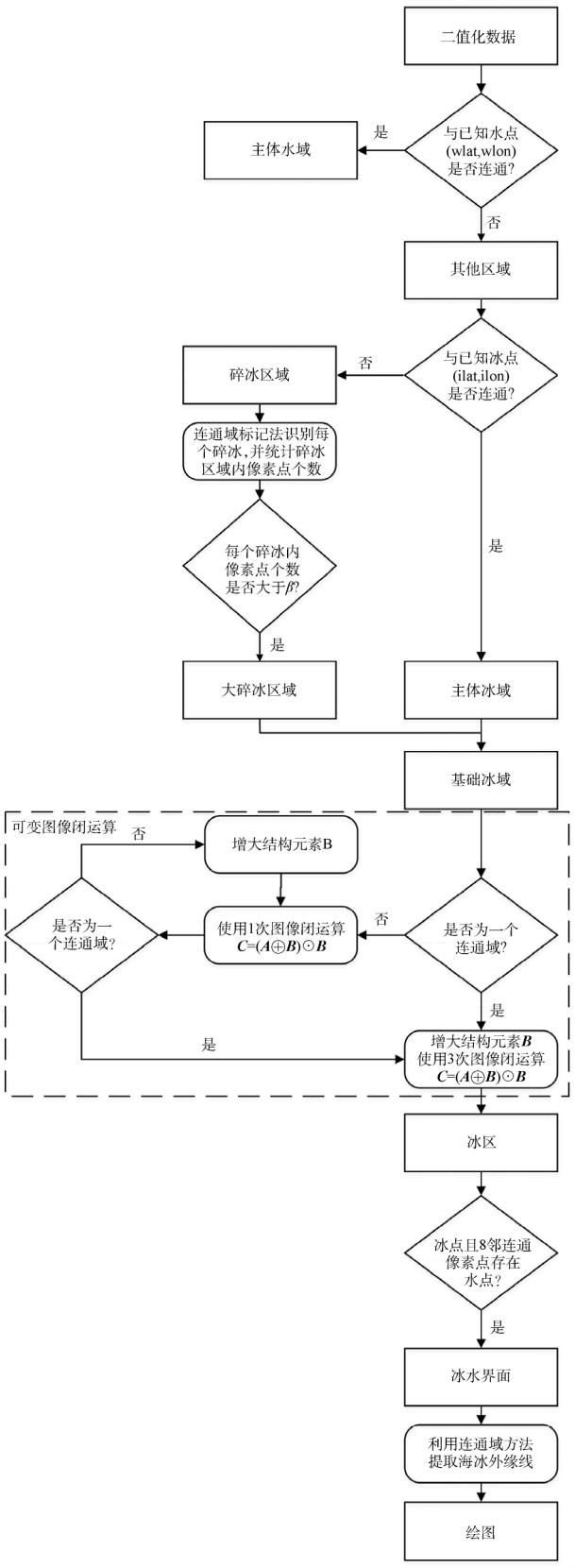

图 3 可变图像闭运算算法提取海冰外缘线的流程图

步骤 2: 确定水域点和冰域点。 选取最高纬度的一个冰点作为冰域点 P_i,选取最低纬度一个水点作为水域点 P_w。

步骤 3: 识别主体水域。 具体是对步骤(1)得到的二值化数据中的 P_w 进行连通域处理,本文采用的是单点连通域标记。与该坐标点连通的点赋值为 1,不连通的点赋值为 0,得到赋值为 1 的点组成的主体水域,如图 4(b)。

步骤 4: 识别主体冰域。 在步骤(3)得到的二值化数据中,对冰域点 P_i 进行单点连通域处理,与该点连通的点赋值为 1,不连通的点赋值为 0,得到主体冰域。具体连通规则与步骤(3)相同。图 4(c)中的白色区域即主体冰域。

步骤 5: 识别碎冰区。 结合步骤(3)的主体水域和步骤(4)的主体冰域二值化数据,将两者数据中相同值的数据点判为碎冰区域。本文中将主体水域和主体冰域中都是 0 的点,判断为碎冰区域,标记为 1,其他区域标记为 0。碎冰区为图 5(d)中的白色点。

步骤 6: 区别大小碎冰区,合并主体冰域,得到基础冰区。 首先,对步骤(5)得到的碎冰区进行区域连通域标记处理,即对步骤(5)得到的每一个碎冰区进行排序。然后计算出每个碎冰区的数据点总数,将总数小于 β 的碎冰区去除,将总数大于等于 β 的较大碎冰区标识为 1,与步骤(4)得到的主体冰区合并,作为基础冰区; 除非在整个图像中没有总数大于等于 β 碎冰区,如果存在 n 个面积大于等于 β 碎冰区,那么基础冰区属于 $n+1$ 个连通域(n 个大的碎冰区和 1 个主体冰域)。本文 β 值选取为 20。上述 MODIS 数据中大于 β 的较大碎冰区的效果图见图 5(d); 基础冰区的效果图见图 4(e),其中基础冰区标记为 1,其他区域标记为 0。

步骤 7: 对基础冰区数据图像进行可变闭运算处理。 步骤(6)得到的基础冰区是二值化数据,对该二值化数据进行可变图像闭运算。具体的计算公式是: $\boldsymbol{C}=(\boldsymbol{A}\oplus\boldsymbol{B})\otimes\boldsymbol{B}$。其中,$\boldsymbol{A}$ 为二值化数据,$\boldsymbol{B}$ 为结构元素,$\boldsymbol{C}$ 为得到的图像矩阵。每循环一次 $\boldsymbol{B}$ 按同样的形式行列分别增加 2,按照图 2 的特征发生变化; 在每进行一次图像闭运算处理后,都对得到的数据进行区域连通域标记处理; 如果连通域标记出只有一个连通域,那么之后再进行 4 次图像闭运算,以平滑曲线; 若否,继续进行图像闭运算处理,直到 $n+1$ 个连通域合并为同一个连通域。得到的唯一的连通域中所有的点赋值为 1,表示整片冰区,其他点赋值为 0,表示水点。

步骤 8: 确定海冰外缘线位置。 对步骤(7)所得

唯一连通域利用8邻域连通方法。如果选择点是冰点,且周围8个点有水点存在,说明该点处于冰水界面上,赋值为1,其他区域(包括水点和界面以外的冰点)都赋值为0。

步骤9:冰外缘线数据输出。将步骤(8)得到的确定海冰外缘线位置数据输出。为了能够具有更好的直观效果,在步骤(9)中,可以首先对步骤(8)获得的二值图像同样进行单点连通域处理,获得海冰外缘线在图像数据中的行列信息,然后保存为bln文件格式的文件进行输出。bln文件格式详情请参考surfer软件说明文档([2014-05-21] http://www.goldensoftware.com/)。上述基于MODIS数据提取得到的海冰外缘线见图4(f)中红线所示。

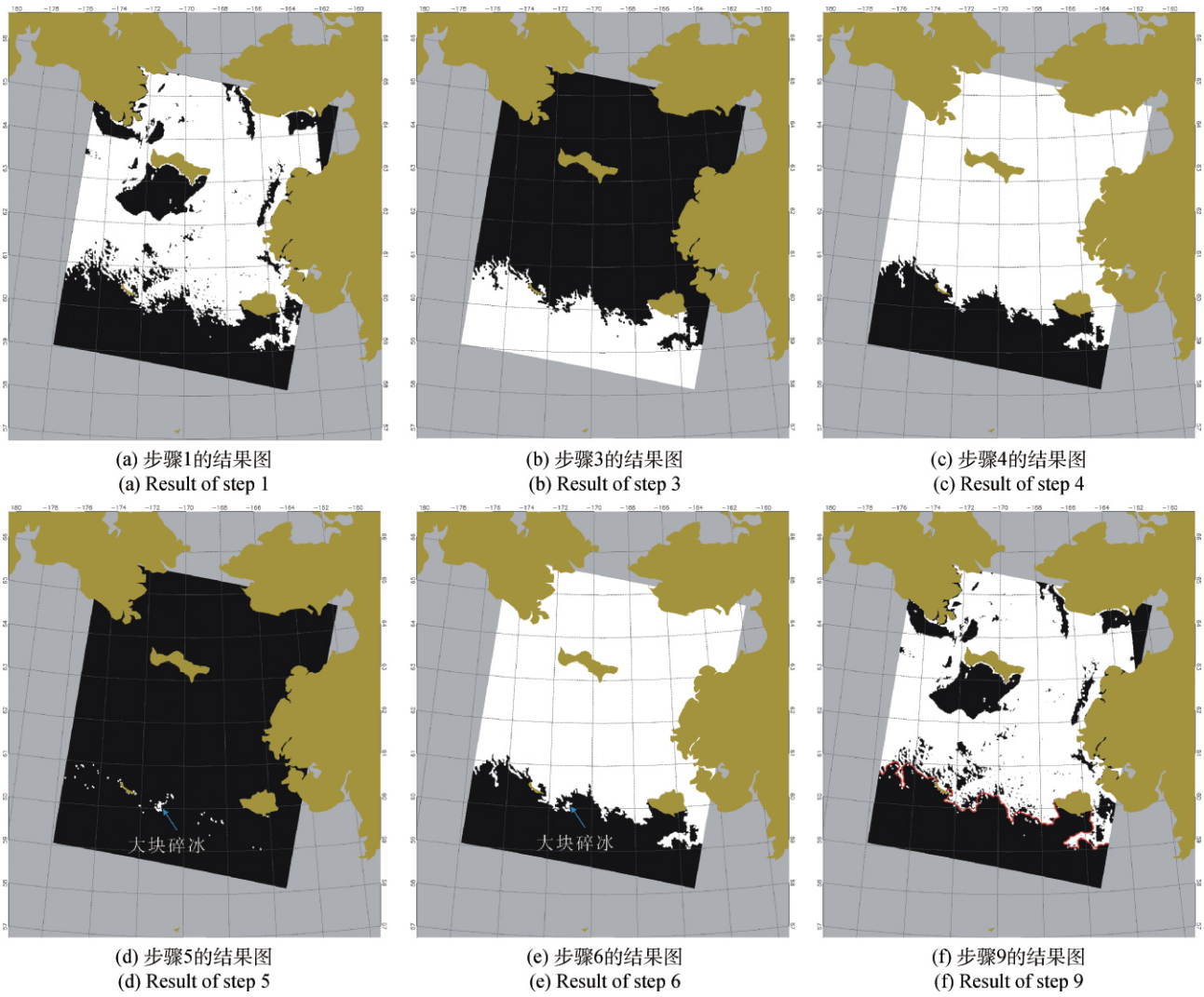

(a) 步骤1的结果图 (a) Result of step 1
(b) 步骤3的结果图 (b) Result of step 3
(c) 步骤4的结果图 (c) Result of step 4
(d) 步骤5的结果图 (d) Result of step 5
(e) 步骤6的结果图 (e) Result of step 6
(f) 步骤9的结果图 (f) Result of step 9

图4 可变图像闭运算方法提取海冰外缘线的过程图

本文提出的海冰外缘线自动提取方法首先采用强度比算法对MODIS图像进行处理,将海冰密集度等数据集进行二值化处理,继而结合连通域算法,分别识别图像中主体冰域和主体水域。在此基础上,再次采用连通域标记方法,选择碎冰区中较大面积的碎冰,并将其与主体冰域合并,得到基础冰区数据。最后使用可变图像闭运算方法对基础冰区数据进行处理,结合连通域标记方法,最终确定海冰外缘线的位置。

3 算法应用及结果分析

本文给出的海冰外缘线提取方法是基于冰水二值场数据,可以方便地应用于各种海冰密集度数据。可以通过设置阈值,将海冰密集度大于阈值的点设为冰点,取值为1,小于阈值的点设为水点,取值为0,建立冰水二值场,应用图3流程提取海冰外缘线。以分辨率为6.25 km的AMSRE海冰密集度

为例,分别给出了阈值为 0%(绿线)和 15%(红线)的冰水二值场,以此获得海冰外缘线,如图 5 所示。

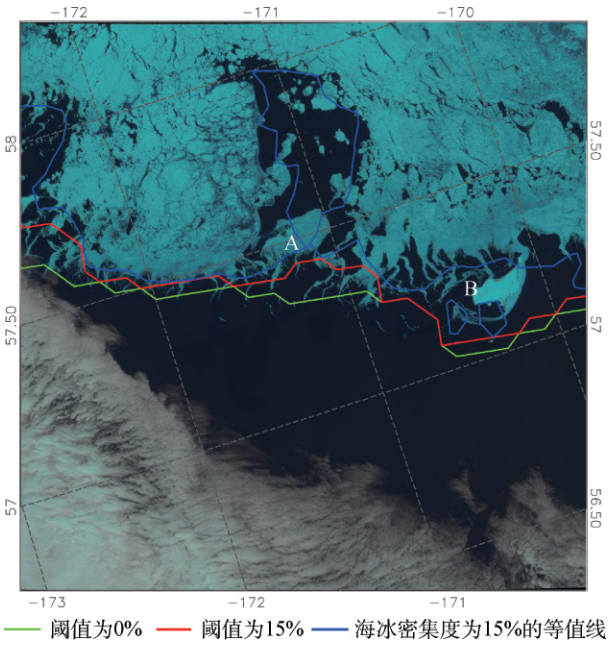

图 5 利用 2013 年 4 月 19 日 AMSRE 海冰密集度数据,分别以阈值为 0% 和阈值为 15% 建立冰水二值场,识别获得海冰外缘线(背景图像为当日的 Landsat 真彩图)

从图 5 中可以看出,在某些区域,将 15% 海冰密集度的等值线视为海冰外缘线是不合理。如图 5 中 *A* 处的冰间水域,此处的等值线被隔断; *B* 处碎冰被单独处理,形成一个个独立的等值线闭环。采用本文提供的方法获得的海冰外缘线,不管是以 0% 还是 15% 作为阈值,都只形成一条外缘线,且在冰间水域处较为合理,在碎冰处没有形成闭环。从中可以看出,以阈值为 0% 计算获得的海冰外缘线远离海冰主体。主要原因是在冰水交界处,特别是在夏季,由于风的作用,往往会出现大量的伸向开阔水域的带状冰域。如果以 0% 作为阈值,识别得到的海冰外缘线是带状冰域终点的连线,这样的海冰外缘线包络了大量的与外海相通的开阔水域。以 15% 作为阈值,运用本文提出的方法,获得的海冰外缘线,相比于海冰密度为 15% 的等值线则最能反映海冰主体范围。

为了更好阐述本文方法提取得到的海冰外缘线的优点,这里,取 15% 作为阈值,建立冰水二值场,应用图 3 流程提取海冰外缘线。以分辨率为 6.25 km 的 AMSR-E 海冰密集度数据(苏洁 等,2013)为例,给出了 10 个不同区域图 6(a)—图 6(j)、不同时间的应用个例。图 6 中特殊区域(包括被大量碎冰区域覆盖的海域,被大块碎冰覆盖的海域和存在冰间水道的海域)用字母加数字标识。例如 E1 区域代表 E 图中被大量碎冰覆盖的区域,E2 区域代表 E 图中被大块碎冰覆盖的区域,E3 区域代表该区域中存在冰间水道。将本文自动提取的海冰外缘线与 15% 海冰密集度等值线比较,可以看出,在碎冰较少的海域(如图 6(c)、(g)、(h)),两者差别很小。在碎冰较多的海域,尤其在海冰密集度变化剧烈的海域,如图 6 中(a)、(b)、(d)、(e)、(f)、(i)和(j)区域,两者相差较大。主要表现在 3 个方面: 1) 如果将 15% 海冰密集度等值线视为海冰外缘线,对包含众多小碎冰区域,以 A1、D1、E1 和 J1 为例。海域中虽包含了众多小连通区域,却都不能反映区域内海冰主体的覆盖范围。本文提出的方法筛选了碎冰区域,将较小的碎冰去除,保留较大的碎冰,得到的海冰外缘线包括众多的碎冰,能反映出该海域海冰的覆盖状况; 2) 对巨大碎冰区域,以 D1、E2、F1、I1 和 J2 区域为例,15% 海冰密集度等值线即为大冰块的外缘,此时远离主体冰域而单独存在。本文提出的海冰外缘线提取算法将这些巨大的碎冰与主体冰域合并,共同提取海冰外缘线,得到的海冰外缘线更加合理; 3) 在有冰间水道区域,如 B1、B2、E3 和 I2 区域,15% 海冰密集度等值线会深入厚冰区。而本文由于使用了图像膨化算法,使得所提取的海冰外缘线在冰间水道口连接,更加符合大尺度海冰范围的概念。

图 5 和图 6 能够直观地给出两种方法得到的海冰外缘线之间的差别,体现了本文海冰外缘线提取算法的优势。同时考虑到 Landsat 数据只覆盖陆地和海岸部分海域,难以提供整个海冰外缘线区域的验证数据。所以本文暂没有量化两种方法得到的海冰外缘线之间的差异。在将来的研究中将考虑使用其他数据进一步计算精度指标。

4 结 论

海冰外缘线能直观地给出海冰分布范围,是海冰变化研究中的重要内容之一,同时也是我国海冰灾害预警启动标准的指标。如何快速、有效且自动地提取海冰外缘线是一个必须解决的问题。为了摒弃人工提取外缘线的主观因素,同时保留尽可能多的碎冰区,本文基于图像处理方法中连通域标记算法和图像闭运算算法,提出了一种基于卫星数据的海冰外缘线自动提取算法。该方法可适用于任何能够提供冰水二值场的数据,包含海冰密集度、海冰卫星图像以及航拍图像。

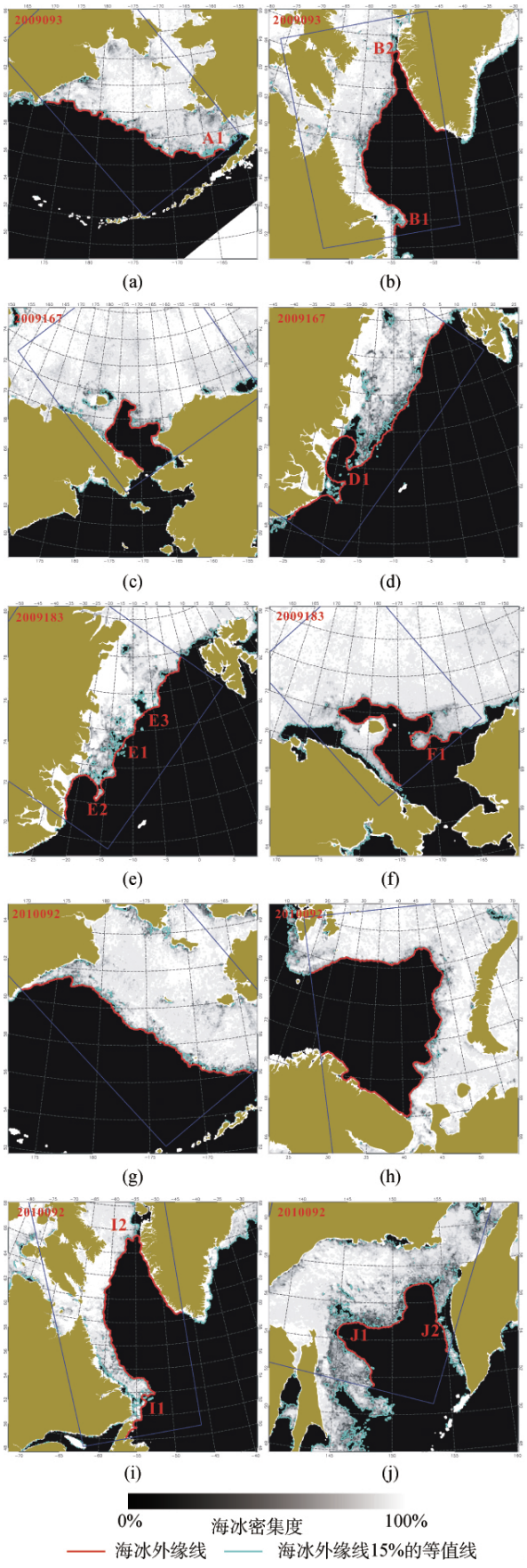

图 6 利用本文方法识别得到的海冰外缘线与海冰外缘线 15% 的等值线的比较(蓝框代表选取的数据范围)

基于 AMSR-E 海冰密集度数据,利用本文方法提取了北冰洋 10 个不同区域、不同时间的海冰外缘线位置信息。与 15% 海冰密集度等值线比较发现,两者在碎冰较少的海域基本一致。在碎冰较多的海域,两者相差很大。由于本文的海冰外缘线提取方法一方面忽略了较小碎冰,另一方面将较大碎冰和主体冰域合并,共同提取海冰外缘线,得到的海冰外缘线对衡量大尺度海冰范围更为合理。

本方法具有完全自动化、快速、操作简单、应用范围广等优点。利用本文方法能快速地为南北极海冰监测提供实时的大范围、长时间尺度的极区海冰外缘线,也能够服务于中国海冰灾害预警预报与研究。

志 谢 感谢郝光华和李彦青提供 AMSR-E 海冰密集度反演数据。

参考文献(References)

Breivik L A, Eastwood S and Lavergne T. 2012. Use of C-Band scatterometer for sea ice edge identification. IEEE Transactions on Geoscience and Remote Sensing, 50(7): 2669 – 2677 [DOI: 10.1109/TGRS.2012.2188898]

程瑶瑶, 史久新, 郑少军. 2012. 南极麦肯齐湾冰间湖的时空变化及主要影响因素分析. 中国海洋大学学报, 42(7/8): 1 – 9

Divine D V and Chad D. 2006. Historical variability of sea ice edge position in the Nordic Seas. Journal of Geophysical Research, 111: C01001 [DOI: 10.1029/2004JC002851]

Drüe C and Heinemann G. 2005. Accuracy assessment of sea-ice concentrations from MODIS using in-situ measurements. Remote sensing of Environment, 95(2): 139 – 149 [DOI: 10.1016/j.rse.2004.12.004]

Fu H L, Zhao J P and Frey K E. 2012. Investigation of polynya dynamics in the northern Bering Sea using greyscale morphology image-processing techniques. International Journal of Remote Sensing, 33(7): 2214 – 2232 [DOI: 10.1080/01431161.2011.608088]

Key J and Haefliger M. 1992. Arctic ice surface temperature retrieval from AVHRR thermal channels. Journal of Geophysical Research: Atmospheres (1984—2012), 97(D5): 5885 – 5893 [DOI: 10.1029/92JD00348]

孔斌. 2003. 快速连通域分析算法及其实现. 模式识别与人工智能, 16(1): 110 – 115

刘成龙, 赵进平. 2013. 夏季北极密集冰区范围确定及其时空变化研究. 海洋学报, 35(4): 36 – 46

Mahoney A R, Barry R G, Smoolyanitsky V and Fetterer F. 2008. Observed sea ice extent in the Russian Arctic, 1933—2006. Journal of Geophysical Research, 113: C11005 [DOI: 10.1029/2008JC004830]

牟龙江, 赵进平. 2013. 格陵兰海海冰外缘线变化特征分析. 地球

科学进展, 28(6): 709 – 717 [DOI: 10.11867/j.issn.1001 – 8166.2013.06.0709]

Ogi M, Rigor I G, McPhee M G and Wallace J M. 2008. Summer retreat of Arctic Sea Ice: role of summer winds. Geophysical Research Letters, 35(24): L24701 [DOI: 10.1029/2008GL035672]

Spreen G, Kaleschke L and Heygster G. 2008. Sea ice remote sensing using AMSR-E 89-GHz channels. Journal of Geophysical Research (Oceans), 113(C2) [DOI: 10.1029/2005JC003384]

苏洁, 郝光华, 叶鑫欣, 王维波. 2013. **极区海冰密集度** AMSR-E **数据反演算法的试验与验证**. **遥感学报**, 17(3): 495 – 513 [DOI: 10.11834/jrs.20132043]

Sullivan C W, McClain C, Comiso J C and Smith W O Jr. 1988. Phytoplankton standing crops within an Antarctic ice edge assessed by satellite remote sensing. Journal of Geophysical Research, 93(C10): 12487 – 12498 [DOI: 10.1029/JC093iC10p12487]

王宁, 张晰, 纪永刚, 鲁统臻, 于波. 2011. **凝聚层次聚类的** MODIS **海冰外缘线提取算法与应用**. **地球信息科学学报**, 13(2): 266 – 272 [DOI: 10.3724/SP.J.1047.2011.00266]

Worby A P and Comiso J C. 2004. Studies of the Antarctic sea ice edge and ice extent from satellite and ship observations. Remote Sensing of Environment, 92(1): 98 – 111 [DOI: 10.1016/j.rse.2004.05.007]

Worby A P, Massom R A, Alllison I, Lytle A I and Heil P. 1998. East Antarctic sea ice: a review of its structure, properties and drift//Jeffries M O, ed. Antarctic Sea Ice: Physical Processes, Interactions and Variability. Antarctic Research Series (Book 74). American Geophysical Union: 41 – 67 [DOI: 10.1029/AR074p0041]

赵进平, 任敬萍. 2000. **从航空数字影像提取北极海冰形态参数的方法研究**. **遥感学报**, 4(4): 271 – 278 [DOI: 10.11834/jrs.20000406]